Climate Dynamics
https://doi.org/10.1007/s00382-021-05875-w

Influence of the Boreal Summer Intra-Seasonal Oscillation on rainfall in the Blue Nile Basin

Zewdu Alamineh Fetene[1,2,5] · Benjamin F. Zaitchik[2] · Tadesse Terefe Zeleke[3] · Baylie Damtie Yeshita[4] · Cristina G. Recalde-Coronel[2]

Received: 1 August 2020 / Accepted: 29 June 2021

Abstract
The drivers of precipitation variability in the Ethiopian Highlands are complex, and they have considerable impact on the local rural economy of the region. While interannual variability has been studied extensively, relatively less study has focused on intra-seasonal variability in precipitation, even though this variability can be critical for agricultural activities. In this study, we examine the impacts of the Boreal Summer Intra-Seasonal Oscillation (BSISO) on precipitation variability in the Upper Blue Nile Basin (UBNB) during the rainy season (June–September). In order to optimally capture Intra-seasonal variability, we developed a customized ISO index based on leading modes of the variability in the UBNB, and found that this index shares the general character of a standard BSISO index. Analyses performed with both the customized and standard BSISO indices show that a core convective region centered on the Indian Ocean propagates to the northwest, eventually exerting significant influence on Ethiopian rainfall. The primary mechanism of influence appears to be BSISO influence on both lower and upper level tropospheric wind fields over the western Indian Ocean that influence moisture flux, convergence, and convection in the study region. This includes BSISO modulation of the East Africa Low-Level Jet and the Tropical Easterly Jet. We also find that the BSISO influence on Ethiopia is consistent with a BSISO-associated Rossby wave signal, but the magnitude of the Rossby wave signal is small relative to other mechanisms of influence.

Keywords Boreal Summer Intra Seasonal Oscillation · Upper Blue Nile Basin Intra Seasonal Index · Intra seasonal variability · Upper Blue Nile Basin · Precipitation

1 Introduction

The Ethiopian Highlands are characterized by significant spatial and temporal climate variability (Conway 2000). This variability is of considerable importance, both because the rural economy of the region depends strongly on rainfed smallholder agriculture and because the highlands are the "water tower of Africa," serving as the headwaters for multiple major rivers, including the Blue Nile River. For the Upper Blue Nile Basin (UBNB), the drivers of interannual variability at basin scale have been the subject of considerable study (e.g., Gissila et al. 2004; Korecha and Barnston 2007; Block and Rajagopalan 2007; Abtew et al. 2009; Diro et al. 2011; Viste and Sorteberg 2011; Zeleke et al. 2013; Nicholson 2017), with much research and operational interest in the influence that the El Niño Southern Oscillation (ENSO), the Indian Ocean Dipole (IOD) and other modes of large-scale climate variability have on summertime (*Kiremt*) rainfall and Blue Nile flow. Spatial variability in climate, and particularly rainfall, within the UBNB is generally understood to be a function of local altitude, latitude, humidity and winds (Zeleke et al. 2017). As rainfall in the region is highly convective in nature, these contrasts influence both mean climate conditions and temporal variability at local scale.

✉ Zewdu Alamineh Fetene
alamineh.zewdu36@gmail.com

1 Atmospheric Physics, Bahir Dar University, Bahir Dar, Ethiopia

2 Department of Earth and Planetary Sciences, Johns Hopkins University, 301 Olin Hall, 3400 N. Charles Street, Baltimore, MD 21218, USA

3 Institute of Geophysics, Space Science and Astronomy, Addis Ababa University, Addis Ababa, Ethiopia

4 Washera Geospace and Radar Science Laboratory, Bahir Dar University, Bahir Dar, Ethiopia

5 Physics, Debre Tabor University, Debre Tabor, Ethiopia

Published online: 13 July 2021

While most studies of temporal climate variability and change in the UBNB have focused on interannual variability in rainfall, subseasonal variability within the *Kiremt* can be substantial, with significant impacts on agricultural livelihoods and enhance the quality of climate forecasting (Berhane et al. 2014; Zaitchik 2017; Eggen et al. 2019). Understanding variability on this timescale, therefore, is important both for the fundamental science of climate variability in the region and for agriculture and resource applications.

When considering variability at subseasonal timescales, particularly in tropical regions, the tropical intraseasonal oscillations (ISOs) offer an important point of entry to reduce risk of natural disaster (Donald et al. 2006). The Madden-Julien Oscillation (MJO; Madden and Julian 1971) is the leading ISO and has a significant impact on rainfall patterns across the global tropics (Jones and Carvalho 2011; Jones 2016). This includes regional impacts on precipitation in South America (e.g., Recalde et al. 2019; Souza and Ambrizzi 2006; Shimizu and Ambrizzi 2016), Indonesia and tropical Australia (e.g., Hidayata and Kizu 2010; Rauniyar and Walsh 2011; Wheeler et al. 2009), and Africa (Zaitchik 2017)—including West Africa (Lavender and Matthews 2009; Berhane et al. 2015), and equatorial East Africa (Pohl and Camberlin 2006; Berhane and Zaitchik 2014)—among other regions. The strength and mechanisms of these impacts vary by season and by region, and include direct influence of the eastward-propagating MJO convective core through a region, synoptic influences of MJO convective activity, and the influence of MJO-associated Kelvin and Rossby waves that propagate eastward and westward from the center of MJO action.

One of the fundamental features of tropical intraseasonal oscillations is the pronounced seasonal variation in their intensity (Madden 1986), movement (Wang and Rui 1990), and periodicity (Hartmann et al. 1992). In particular, the boreal summer ISO (BSISO) exhibits several fundamental characteristics that distinguish it from the MJO found in other seasons, and these differences are critical when considering ISO-related rainfall variability during the summertime Kiremt rainy season. The MJO is classically defined as an equatorially trapped, eastward propagating convectively coupled Kelvin wave (Madden and Julian 1972). The MJO lifecycle is thus conveniently described in terms of phases that are defined by the position of the convective core across the tropical longitude (Zhang 2005; Hsu and Li 2012; Wang et al. 2012; DeMott et al. 2015; Zaitchik 2017). In contrast, the BSISO exhibits prominent northward propagation in the monsoon regions (Yasunari 1979; Krishnamurti and Subrahmanyam 1982; Chen et al. 2016) and a significant standing oscillation component between the equatorial Indian Ocean and the tropical western North Pacific (Zhu and Wang 1993). It also features a northwest-southeastward tilted rainband (Ferranti et al. 1997; Wang and Xie 1997). It has complex structures in time and space owing to its interaction with the mean monsoon circulation (Webster et al. 1998; Lau and Waliser 2005; Wang et al. 2005), and the mean state moist static energy distribution (Wang and Xie 1997).

Though BSISO teleconnections are not as widely studied as MJO in other seasons, the BSISO has been implicated in the modulation of tropical cyclones across the tropics, including the Indian, northwest Pacific, northeast Pacific, and Atlantic Ocean (Liebmann and Smith 1996; Maloney and Kiehl 2002; Higgins and Shi 2001; Klotzbach 2014). More generally, BSISO (or, sometimes "summertime MJO") impacts on precipitation events have been documented in Asia (Zhu et al. 2003; Mao and Wu 2006; Yang et al. 2010; Lee et al. 2012; Chen et al. 2015; Hsu et al. 2016), and further afield, the BSISO produces a significant variability in West African summertime rainfall (Matthews 2004; Mohino et al. 2012) via easterly wave activity. Zaitchik (2017) reviews some studies that consider ISO influence on East African summertime rainfall, but those studies use MJO rather than BSISO indices and do not investigate mechanism. To our knowledge, no study has quantified or explained the influence of BSISO on the UBNB during its summertime rainy season.

2 Methods of analysis

2.1 Study area

The UBNB is located in northwestern Ethiopia and covers a drainage area of 175,000 km^2, extending from the escarpment of the Rift Valley in the east to the Sudanese border in the west and from the Lake Tana basin in the North down

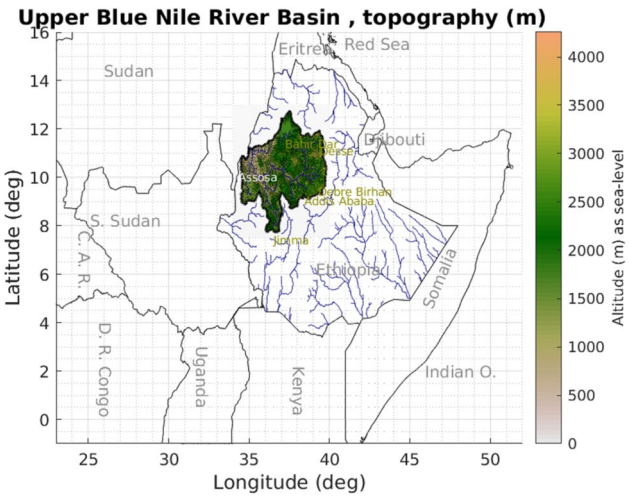

Fig. 1 The location of UBNB (green shaded region)

to Ambo River basin in the South (see Fig. 1). The UBNB's elevation ranges from 350 m asl near the Sudanese border to 4230 m asl in the central part of the basin (Betrie et al. 2011; Taye and Willems 2012). The climate of the basin varies significantly according to altitude, with annual rainfall ranging from 400 mm near the Ethiopia–Sudan border to 2200 mm in the Didesa and Dabus sub-basins. Rainfall peaks in summer, in concert with the seasonal migration of the Inter-Tropical Convergence Zone, or ITCZ (Mellander et al. 2013; Zeleke et al. 2013). These summertime (June-September) *Kiremt* rains are by far the dominant source of precipitation in the UBNB. The eastern part of the basin does also receive spring Belg rains (February to May), but summer rains are larger, and the western part of the basin has a unimodal summer rainfall regime. The Blue Nile River discharge regime is highly seasonal, with over 80 % of its annual discharge occurring from July to October, and only 4 % from January to April (Kim and Kaluarachchi 2009; Sutcliffe and Parks 1999). The Blue Nile is the largest tributary of Nile River, contributing from 60 to 70 % of the total annual flow of the main Nile (Nawaz et al. 2010).

2.2 Data and analysis

Daily outgoing longwave radiation (OLR) data are obtained from the Advanced Very High-Resolution Radiometer (AVHRR) onboard the National Oceanic Atmospheric Administration (NOAA) polar-orbiting satellites for the period of 1983–2018 (35 year) and are used as a proxy for deep convection (e.g., Nogués-Paegle et al. 2000; Lee et al. 2012). Daily precipitation estimates are drawn from the Climate Hazards InfraRed Precipitation with Stations (CHIRPS) product, v2. CHIRPS is a blended product that combines thermal infrared observations from geostationary satellites and in-situ rainfall observations from Global Telecommunications system (GTS) and other sources (Funk et al. 2015; Knapp et al. 2011). CHIRPSv2 offers monthly, pentad and daily products at 0.05 ° resolution for all land areas from 50 °S to 50 °N and is available from 1981 to present. The CHIRPS product is effective for investigating precipitation variability because of its high resolution, 37-year record, easy access, and overall good performance in the tropics, and specifically East Africa (e.g., Dinku et al. 2018).

Daily estimates of BSISO phase and intensity are defined using the bimodal ISO index (Kikuchi et al. 2012; http://iprc.soest.hawaii.edu/users/kazuyosh/Bimodal_ISO.html). This index is designed to capture the off-equatorial character of the BSISO, as compared to the equatorially trapped signal of the MJO that is the target of widely used MJO ISO indices like the Real-time Multivariate MJO (RMM) index developed by Wheeler and Hendon (2004). The bimodal ISO indices of Kikuchi et al. (2012) are calculated based on Extended Empirical Orthogonal Function (EEOF) coefficients (principal components, PCs hereafter) of the Boreal Summer Intra-Seasonal Oscillation modes for combined daily mean OLR and 850-hpa zonal wind anomaly fields averaged over the Asian monsoon region (10 °S–40 °N, 40°–160 °E). Kikuchi et al. (2012) noted that northward/northwestward propagation predominates over eastward propagation during boreal summer, in contrast to other seasons in which the eastward propagation signal dominates. The strength and the phase of ISO is calculated by combining the first two PCs (Lee et al. 2012).

While the bimodal ISO index for boreal summer (for brevity, referred to hereafter as the "BSISO index") provides useful monitoring of the summertime ISO, it is generally recognized that standard ISO indices cannot optimally capture intraseasonal variability in all regions. For this reason, the Climate Variability and Predictability MJO Working Group (Waliser et al. 2008) has recommended that researchers derive a customized ISO based on leading modes of intraseasonal variability in the region of interest. For this study, therefore, we define an UBNB Intraseasonal Index (UISI) to complement the standard BSISO index. The UISI is defined as the first PC of the 30–90-day bandpass filtered gridded OLR anomaly field for the region 7.5–12.5 °N, 35.0–41.5 °E, which corresponds to the Ethiopian Highlands, for June-September. The choice of a 30–90 day bandpass filter is informed by previous work on ISO indices (e.g., Wheeler and Kiladis 1999; Kemball-Cook and Wang 2001; Teng and Wang 2003; Jiang et al. 2004; Lee et al. 2012). The first PC is deemed adequate to capture intraseasonal variability in the filtered OLR anomalies because it accounts for 58.6 % of the total variance and is well separated from the second and third PCs (12.7 and 8.5 %, respectively). Analyses performed with UISI are compared to analyses that use the standard BSISO index in order to assess whether the two indices capture similar atmospheric patterns. All analyses are performed using 35 years of data, 1983–2018 (Fig. 2).

Associations between the intra-seasonal indices (BSISO and UISI) and UBNB precipitation are studied through correlation maps and composites. BSISO composites were made by averaging the filtered daily anomaly fields on the dates when the BSISO amplitude was greater than 1 in the phase of interest, a thresholding approach that is consistent with that used in previous BSISO index studies (Lee et al. 2012). For UISI, we defined positive and negative phases as days when PC1 was higher or lower than one standard deviation ($\pm 1\sigma$) of the PC1 time series, respectively. This thresholding approach is commonly used when an EOF-based index is used to describe an ISO (Kikuchi and Takayabu 2003; Wheeler and Hendon 2004). Thus, UISI composites for the different fields correspond to the average of filtered daily anomalies that fall within the dates of positive or negative phase given by the UISI.

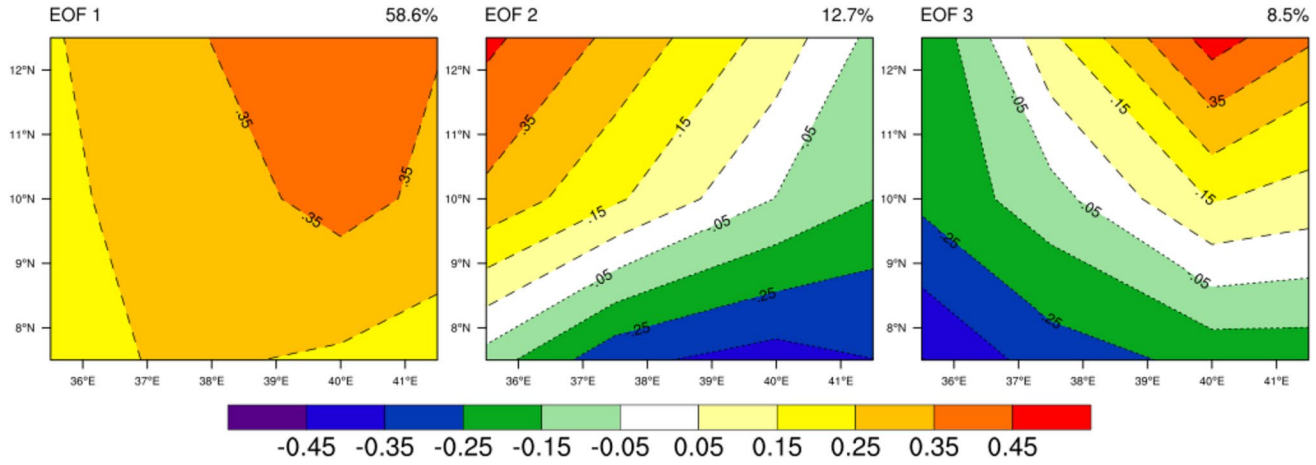

Fig. 2 Spatial structure of the three leading EOF modes of the 30–90-day bandpass filtered OLR data over UBNB (7.5–12.5 °N, 35.0–41.5 °E) for JJAS about 1983 to 2018

In addition, we calculate percentage changes in the probability distribution function of rainfall as:

$$\Delta P_{BSISO} = \frac{P_{BSISO}\left(x \geq x_c\right) - P_{all}\left(x \geq x_c\right)}{P_{all}\left(x \geq x_c\right)} \times 100$$

Where ΔP_{BSISO} is the percentage change in the cumulative probability of rainfall (x) exceeding a given threshold x_c due to the BSISO. P_{BSISO} is the cumulative probability that the rainfall exceeds the threshold calculated for only the days of the given BSISO (or UISI) phases and $P_{all}$is for all days in the summer season.

3 Results and discussion

3.1 Life cycle of the BSISO andits link with UBNB rainfall

The life cycle of the BSISO can be visualized in terms of OLR composited by BSISO index phase (Fig. 3). Here we show the core BSISO development and propagation region centered on the Indian Ocean, but extend the plots to include all of tropical Africa. These composites are constructed using all summertime days that have a BSISO index amplitude greater than one. The general features of BSISO evolution are: in BSISO phase 1 deep convection anomaly is centered over the equatorial Indian Ocean; in phase 2 and phase 3 convection becomes more intense and expands over all of the Indian Ocean and Maritime continent, while the convective center spreads northward; in phase 4 and phase 5 the convective center is positioned over peninsular India, and the equatorial Indian Ocean enters a period of suppressed convection; in phase 6 and phase 7 the suppressed convection anomaly extends to and is eventually concentrated in the Bay of Bengal and South China Sea; in phase 8 convection begins to redevelop in the central equatorial India Ocean (Lee et al. 2012; Ren and Ren 2017).

While the most pronounced direction of zonal propagation is eastward, there is also a clear signal of OLR anomalies propagating northwest from the central Indian Ocean. This direction of propagation is consistent with the Rossby Wave response to equatorial heating (Gill 1980) that has been characterized extensively in studies of MJO dynamics (Wheeler and Kiladis 1999). In the case of the summer monsoon season, however, some of the signal seen to the northwest of the equatorial Indian Ocean, including in our East African study region, is also consistent with synoptic circulations associated with South Asian monsoon variability. The coherent variability in deep convection seen in India and the UBNB, for example (most notably phase 1 and 8 (suppressed) and phase 4 and 5 (enhanced); Fig. 3), resembles associations on interannual timescales have been attributed to variability in the Somali Low Level Jet or the Tropical Easterly Jet (Viste and Sorteberg 2011; Gleixner et al. 2017; Zeleke et al. 2017). This will be explored further in Sect. 3.3. Given the similarities in UBNB response to BSISO phases 4 and 5 and BSISO phases 1 and 8, we combine these two phases in all subsequent BSISO index composites (Fig. 4).

As noted in the Methods section, regionally customized ISO indices can provide more powerful analysis than standard indexing systems when studying regional climate impacts. OLR composites generated using our regionally customized UISI index (Fig. 5) show that the general pattern across the Indian Ocean, South Asia, and East Africa is similar to that found for BSISO (Fig. 4), but with a stronger signal in East Africa.

A positive UISI (Fig. 5) is associated with strong convection in the equatorial Indian Ocean and anomalously dry

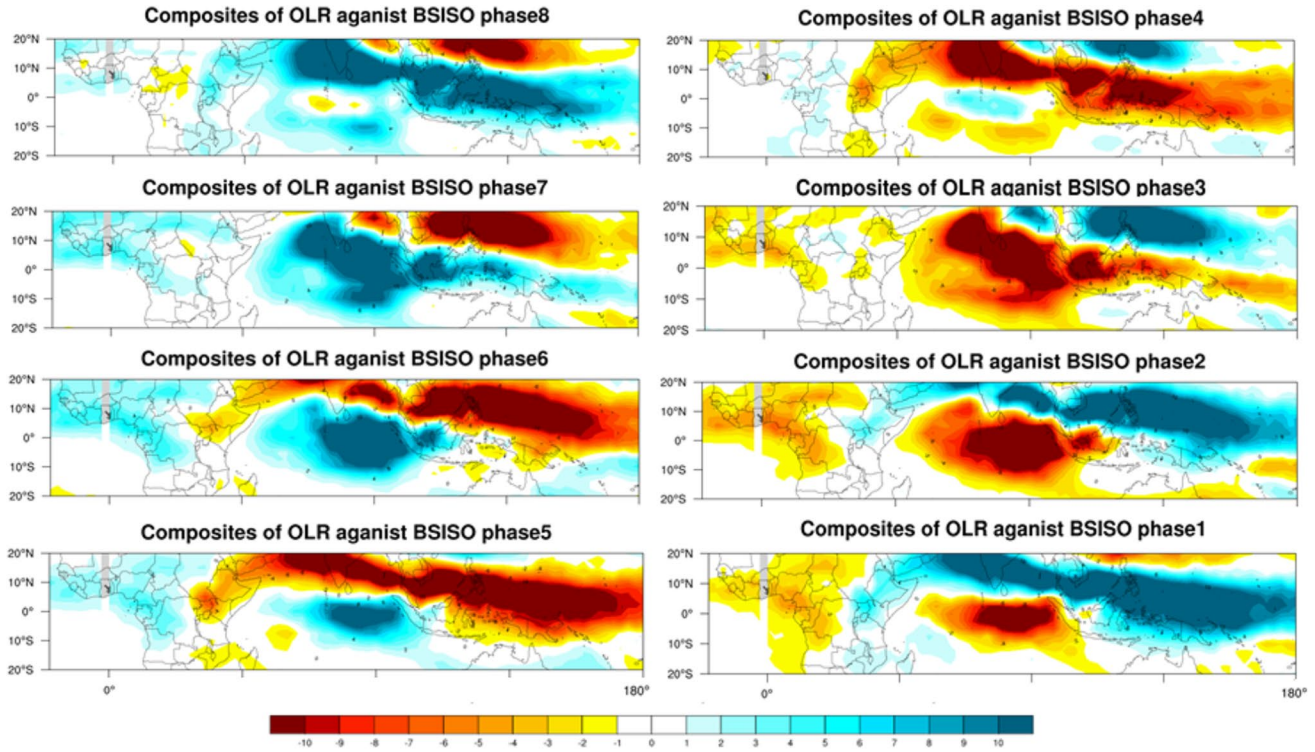

Fig. 3 Life cycle composites of filtered OLR for all phases of the BSISO index, JJAS data, 1983–2018, for all days with BSISO index magnitude > 1

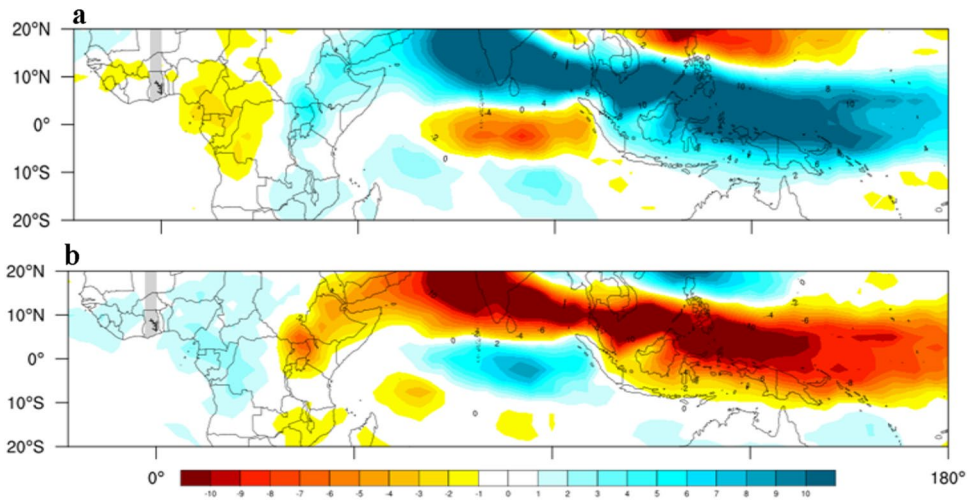

Fig. 4 Combined BSISO phase composites for filtered OLR: **a** phases 1 and 8, associated with suppressed convection in the UBNB; **b** phases 4 and 5, associated with enhanced convection in the UBNB

conditions in East Africa (including the UBNB), across the Arabian Peninsula and Arabian Sea, and all of peninsular India. A negative UISI (Fig. 5) shows the opposite pattern, with anomalously wet conditions in East Africa, the Arabian Sea, and India, and suppressed convection in the equatorial Indian Ocean. The UISI and BSISO composites do not capture identical populations of days, but there is a tendency for BSISO to be in phase 8 or 1 during UISI positive events (52 % of all UISI positive days; phase 8 most common) and, somewhat less conclusively, phase 4 or 5 during negative events (30 % of all UISI positive days; phase 5 most common). Moreover, the evolution of large scale OLR fields prior to and after a UISI positive (negative) event resemble those of BSISO phases prior to phase 1 and 8 (phase 4 and 5) events, suggesting that the UISI captures a regional response to BSISO-related dynamics (Fig. 6).

To quantify the relative contributions of the convectively coupled waves to the BSISO association with

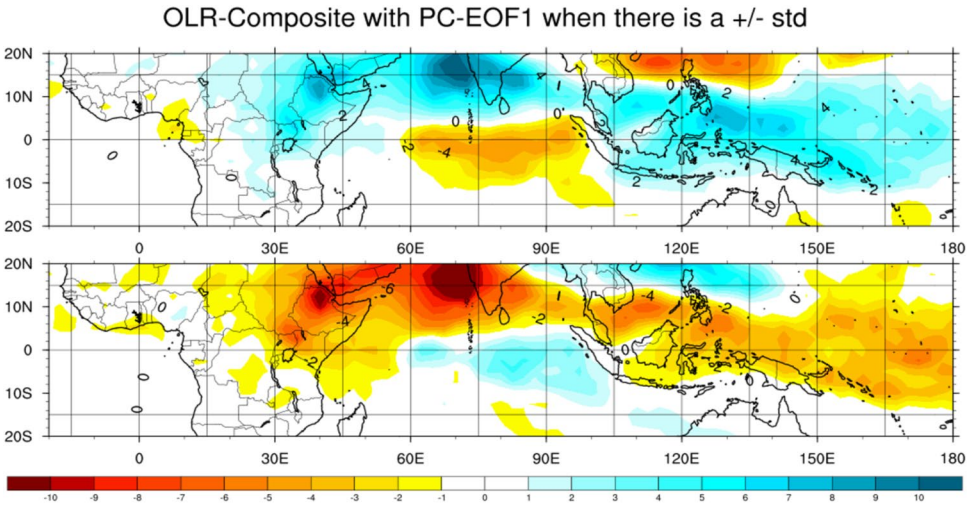

Fig. 5 Composites of filtered OLR against PC-EOF1 (UISI) for JJAS (1983–2018)

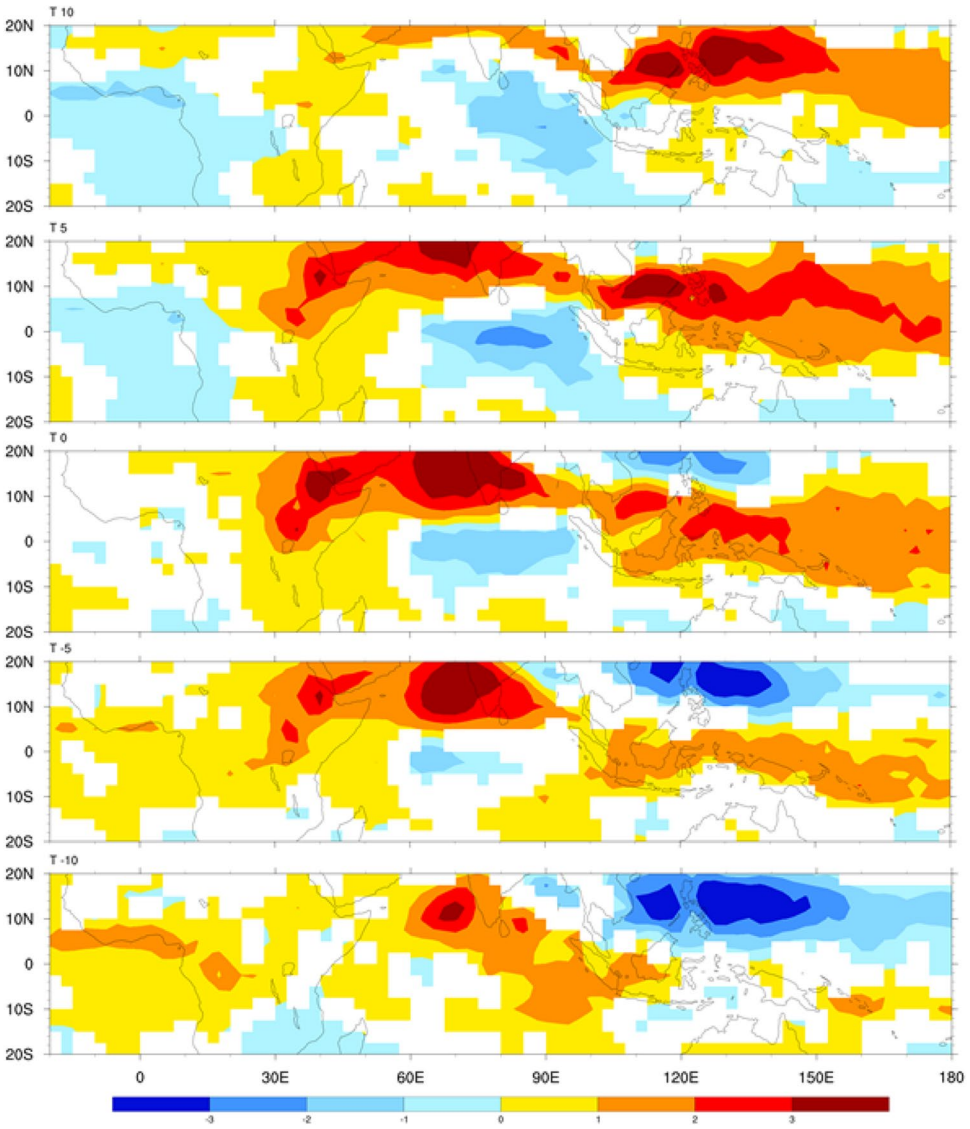

Fig. 6 Time lagged regression coefficients for raw OLR against PC-EOF1 for JJAS, 1983–2018. The shading indicates values significant at 95 confidence intervals

UBNB convection and to compare the strength of the impacts of these waves, we present regression of UISI against OLR filtered to the characteristic wavenumber and frequency of BSISO. The following figures retain much of the signal, and indicate that a considerable amount of the BSISO influence on UBNB summertime precipitation is directly attributable to the migration of the BSISO convention center.

In Fig. 6, time T0 refers to the zero lag correlation between UISI and OLR, negative lags refer to correlations with OLR leading UISI, and positive lags refer to correlations for OLR lagging UISI. The progression in Fig. 6 shows a northward migration of positive OLR anomalies (i.e., suppressed convection) from the equatorial Indian Ocean up into Peninsular India and the Arabian Sea, with strong suppressed convection appearing in East Africa from T-5 through T + 5. This is similar to what we see for BSISO phases 3 through 6, with T0 resembling the phase 4–5 composite shown in Fig. 4.

3.2 The impact of BSISO on precipitation

While OLR is a useful proxy for deep convection, it is important to examine actual impacts on observed precipitation. Composites of precipitation in Fig. 7 are, indeed, consistent with the OLR results we found in Figs. 4 and 5, with reduced rainfall across the core of the Ethiopian Highlands found in BSISO phases 1 & 8 (UISI positive) and enhanced rainfall found in BSISO phases 4 and 5 (UISI negative). These anomalies are approximately 0.5-2.0 mm/day for BSISO and are somewhat larger (up to ~ 3 mm/day) for UISI. To put that magnitude in context, positive UISI is associated with local decreases of precipitation ranging from 0 to 30 % over the UBNB, and up to 50 % or more in parts of southern and southeastern Ethiopia.

The UISI and BSISO indices are calculated using 30–90 day filtered OLR, so by design they capture intra-seasonal rather than interannual variability. That said, it is known that ISO behavior can be impacted by slowly

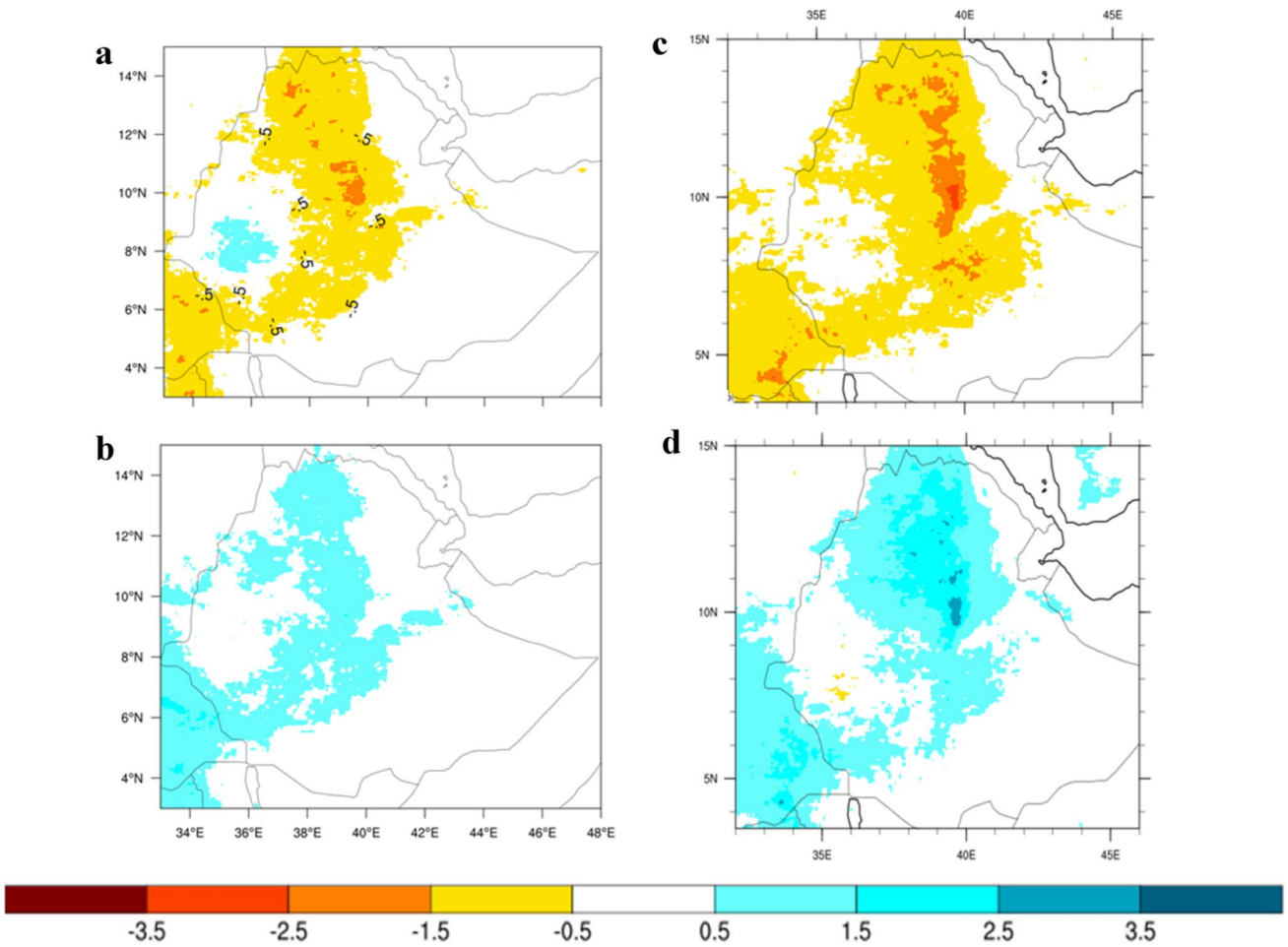

Fig. 7 Composites of precipitation anomalies (mm/day) against BSISO and UISI for JJAS. BSISO composites are for (**a**) phases 1 and 8 with amplitude greater than 1, and (**b**) phases 4 and 5 with amplitude greater than 1. UISI composites are for standard deviation (**c**) greater than 1 and (**d**) less than 1

evolving climate modes, most notably ENSO (Lo and Hendon 2000; Wheeler et al. 2009), such that the frequency of BSISO phases (or UISI events) and the link between BSISO and East Africa might differ according to ENSO phase. For this reason we examine the relationship between Ethiopian precipitation and UISI for La Niña, El Niño, and ENSO-neutral years, to assess whether these patterns are consistent across ENSO state (Fig. 8), using the June-September Oceanic Niño Index (ONI) as the basis for composites. The analysis period includes 17 ENSO-neutral, 11 La Niña and 7 El Niño years. The analysis shows that the sign and spatial pattern of UISI-precipitation composites are generally consistent across ENSO state. Not surprisingly, the magnitude of impact is greatest in La Niña years and smallest in El Niño years, in absolute terms, as La Niña years tend to be wet in this region while El Niño years are dry. The ENSO neutral composites closely resemble the all-year composites (Fig. 7). Based on these results, we proceed with all-years analysis for the remainder of the paper.

3.3 Mechanism of BSISO influence on the UBNB

Rossby waves play an important role in ISO dynamics and teleconnections (Wheeler and Kiladis 1999; Wang et al. 2016; Lin et al. 2019). Kemball-Cook and Wang (2001) diagnosed Rossby Waves associated with the BSISO that propagate north into the Arabian Sea but did not show any evidence of westward wave propagation into Africa. Nevertheless, as we are concerned with influences observed to the northwest of the equatorial Indian Ocean convection center, it is worth considering a potential Rossby wave dynamic. To do this, we apply wavenumber-frequency filtering for Equatorial Rossby wavenumber 1, as described in Wheeler and Kiladis (1999), and examine time-lagged correlation of Rossby-filtered OLR with UISI (Fig. 8), as was shown in Fig. 6 for raw OLR. The pattern of OLR anomaly propagation is, as expected for such a filtered OLR field, consistent with westward propagating equatorial Rossby waves symmetric about the equator. The filtered OLR anomalies are also sign-consistent with the observed influence of BSISO on East Africa, with statistically significant negative OLR anomalies found in East Africa at lag-0. The magnitude of the Rossby-filtered anomalies, however, is small relative to the total OLR anomalies associated with UISI and its BSISO-like OLR correlation patterns. This suggests that Rossby wave induced suppression of convection (or enhancement for -UISI) is, at most, a secondary mechanism for BSISO influence on East African summertime rainfall

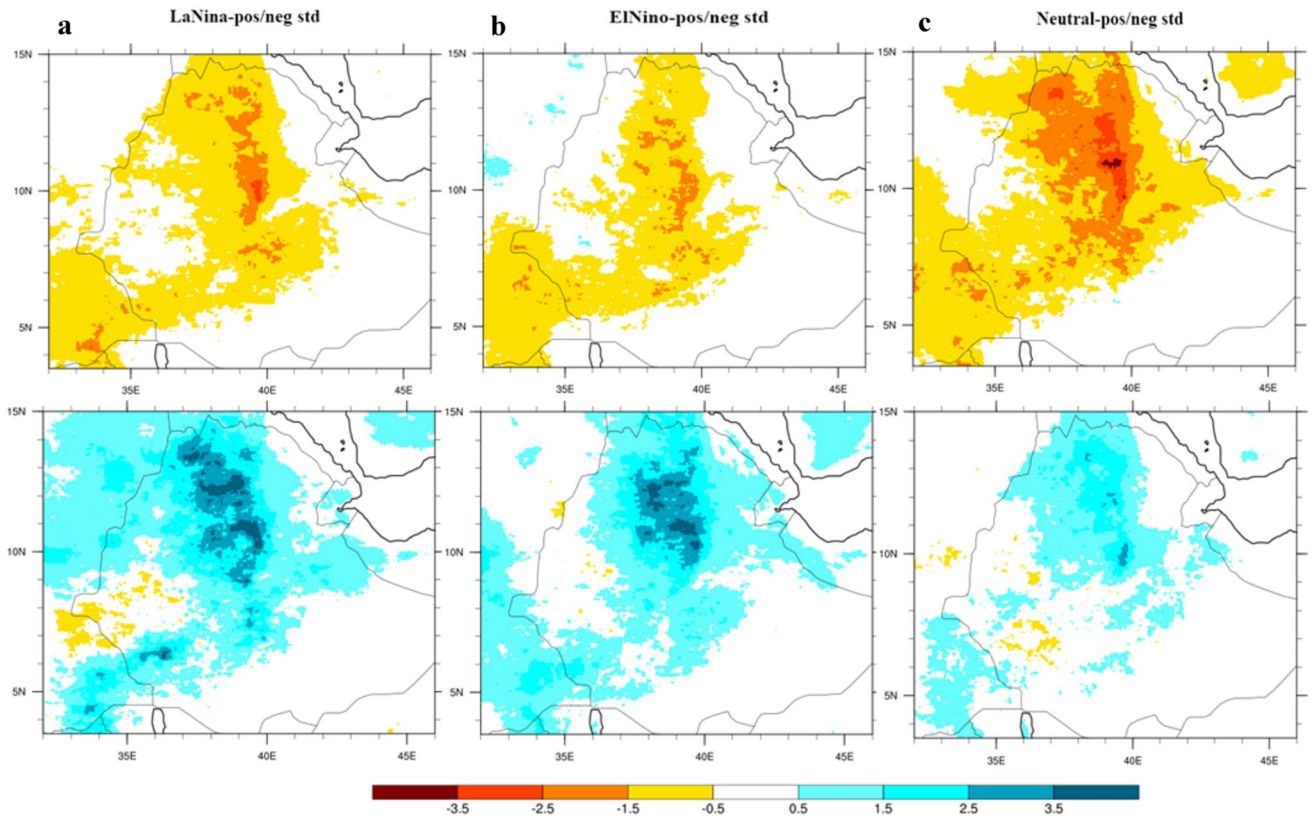

Fig. 8 Composites of daily precipitation anomalies (mm/day) during **a** ENSO-La Niña **b** ENSO-El Niño and **c** ENSO-Neutral years from 1983–2018 against UISI > + 1σ (PC-positive) and UISI < -1σ (PC-negative) for JJAS

(Fig. 9). We note that OLR filtered to free Kelvin Wave wavenumber-frequencies showed very little signal (results not shown).

Next, we consider a potential synoptic link, in which BSISO influence on convection in the South Asian monsoon zone might influence East African atmospheric conditions, particularly via modulation of the East African Low-Level Jet (EALLJ; also referred to as the Somali Jet) or the Tropical Equatorial Jet (TEJ). Figure 10 shows composites of winds (vectors) at 850 hPa and 200 hPa for UISI positive and negative, displayed on a background (shading) of composite windspeed at those levels. At 850 hPa for UISI positive (Fig. 10a), vectors point southwest in the core of the EALLJ off the coast of the Horn of Africa, indicating a weakening of this southwesterly wind feature. While a strong EALLJ is associated with dynamically-induced subsidence along the coast of the Horn of Africa, these winds bring moisture to interior highland Ethiopia through two proposed mechanisms. First, a strong southwesterly jet north of the equator is associated with stronger northeasterly winds that enter

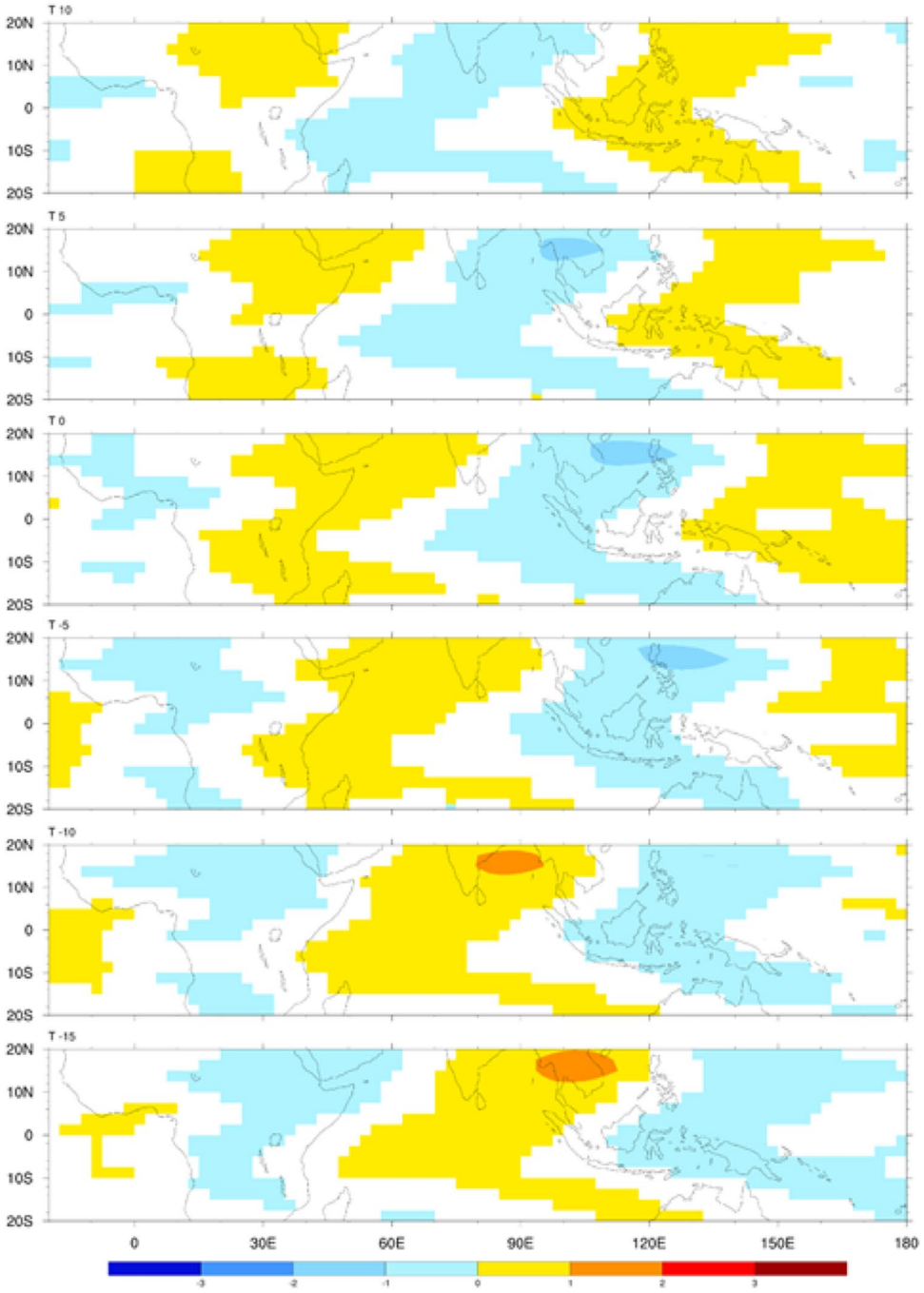

Fig. 9 Rossby wave of OLR anomalies using lag regression against PC-EOF1 for JJAS. The shading indicates values significant at 95 % confidence

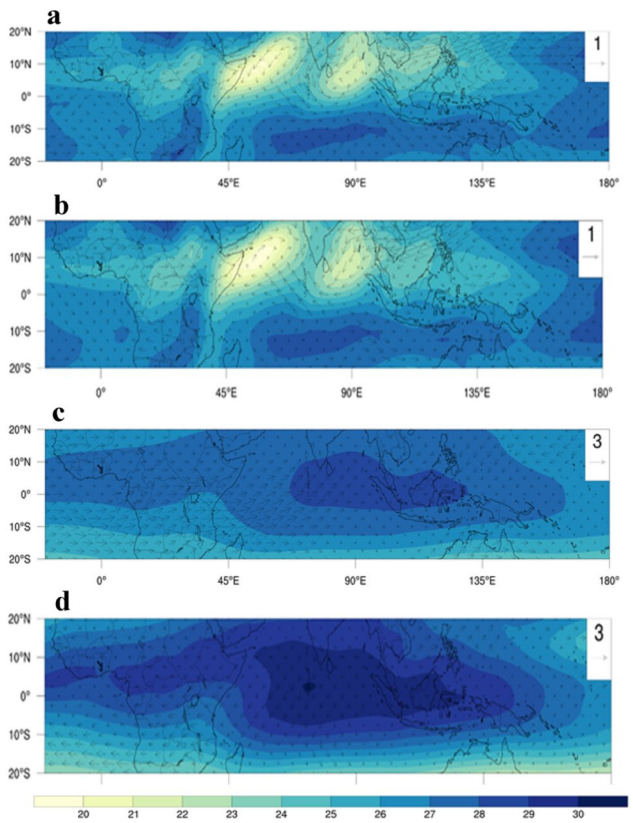

Fig. 10 UISI composite wind speed (shading) and wind anomalies (vectors), calculated for 1983–2018: **a**, **b** 850 hPa winds for UISI **a** positive and **b** negative; **c**, **d** 200 hPa winds for UISI **a** positive and **b** negative

the Horn of Africa from the Indian ocean to the south of the Ethiopian Highlands. These moist winds bring moisture to the highlands and enhance convergence. Second, stronger southwesterly winds off the coast of Ethiopia can enhance the intrusion of low level westerly winds into the Ethiopian Highlands via the Congo Air Stream, which brings moisture-rich air into the Ethiopian Highlands, where topographically-aided ascent leads to precipitation. For these reasons, a weakening of the jet, as seen in Fig. 10a, would be expected to lead to reduced rainfall; indeed, there is evidence of weakened westerlies across central Africa in Fig. 10a, and to a lesser extent signs of weakened northerly flow in from the Indian Ocean. The opposite pattern is seen for UISI negative (Fig. 10b), indicating a strengthened EALLJ, with evidence of increased westerly flow into the Ethiopian Highlands and some sign of enhanced inflow from the Indian Ocean south of the jet.

At 200hpa, there is evidence of a weaker TEJ for UISI positive, with reduced wind speed in the TEJ exit region over Africa (Fig. 10c). The opposite is seen for UISI negative (Fig. 10d). These patterns are consistent with studies of TEJ-mediated ENSO influence on East Africa (Gleixner et al. 2017), which propose that reductions in upper level divergence in the jet exit region under weakened TEJ conditions lead to reduced convection in the Ethiopian Highlands.

4 Conclusions

The importance of tropical Intra-seasonal oscillations (ISO) to precipitation in East Africa has been recognized in a number of previous studies. Those studies, however, have focused on the influence of the Madden-Julien Oscillation (MJO) on equatorial spring and fall rains. In boreal summer, when the Ethiopian Highlands receive the majority of their rains, the ISO has seasonally specific summertime characteristics, and is referred to as the Boreal Summer ISO (BSISO). This study examines the influence of the BSISO on Upper Blue Nile Basin (UBNB) summer precipitation and shows significant associations. We find that during BSISO phases 1 and 8, which we characterize with a regionally customized UBNB Intra-seasonal index (UISI), there is suppression of precipitation in the UBNB, and in phases 4 and 5 (UISI negative phase) there is enhanced precipitation. We find that this pattern is consistent with BSISO patterns of influence and propagation sequences. Mechanistically, we see some evidence of a Rossby wave mediated teleconnection, but the majority of the signal appears to be associated with BSISO influence on wind fields over the Indian Ocean.

This investigation opens opportunities for several areas of follow-on work. First, as sub-seasonal rainfall variability can be critical to crop production in the agriculturally dependent Ethiopian Highlands (e.g., Eggen et al. 2019), information on BSISO activity and, potentially, BSISO-informed subseasonal forecasts could be of value for agricultural management and food security analysis. Second, we observe that the BSISO influence on rainfall is consistent across ENSO phases. While the magnitude of impact during El Niño is somewhat smaller than La Niña, consistent with generally drier conditions during El Niño, the impact of the influence during El Niño-induced droughts could be quite significant, and will depend on the character of BSISO activity during El Niño events. Future studies can examine the role of BSISO activity during UBNB drought periods. Finally, though we have diagnosed mechanisms of influence in this study, we have done so through study of reanalysis fields rather than through controlled modeling experiments. A more robust, model-informed study of BSISO teleconnections could strengthen and expand upon these findings.

Acknowledgements The authors would like to express their sincere gratitude and appreciation to the Department of earth and Planetary Science, John Hopkins University for hosting the first author as a visiting student and Physics Department, Bahir Dar University for their collaborations with the first author during his travel. This research

was supported by U.S. National Science Foundation (NFS) award ICER-1624335.

Author contributions ZAF: Conceived and design the experiments; Conceptualization, Methodology, Investigation, Formal analysis, wrote the paper. BFZ: Writing–review and editing original draft, Fund acquisition, Resources, Conceptualization, Methodology, Investigation, Supervision, Project administration. TTZ and BDY: Supervision–review, writing and editing. CGRC: Resource, review, writing and editing.

Declarations

Conflict of interest The author declares no conflict of interest.

References

Abtew W, Melesse AM, Dessalegne T (2009) El Nino Southern Oscillation link to the Blue Nile River basin hydrology. Hydrol Process 23:3653–3660. https://doi.org/10.1002/hyp.7367

Berhane F, Zaitchik B (2014) Modulation of daily precipitation over east Africa by the Madden–Julian oscillation. J Clim 27:6016–6034

Berhane F, Zaitchik B, Badr HS (2015) The Madden–Julian Oscillation's influence on spring rainy season precipitation over equatorial west Africa. J Clim 28:8653–8672

Betrie GD, Mohamed YA, van Griensven A, Srinivasan R (2011) Sediment management modelling in the Blue Nile Basin using SWAT model Hydrol. Earth Syst Sci 15(3):807–818

Block P, Rajagopalan B (2007) Interannual variability and ensemble forecast of upper Blue Nile Basin Kiremt season precipitation. J Hydrometeorol 8:327–343

Chen J, Wen Z, Wu R, Chen Z, Zhao P (2015) Influences of northward propagating 25–90-day and quasi-biweekly oscillations on eastern China summer rainfall. Clim Dyn 45(1–2):105–124. https://doi.org/10.1007/s00382-014-2334-y

Chen X, Ling J, Li C (2016) Evolution of the Madden–Julian Oscillation in two types of El Niño. J Clim 29:1919–1934

Conway D (2000) The climate and hydrology of the Upper Blue Nile River. Geogr J 166(1):49–62

De Souza EB, Ambrizzi T (2006) Modulation of the intraseasonal rainfall over tropical Brazil by the Madden Julian oscillation. Int J Climatol 26:1759–1776. https://doi.org/10.1002/joc.1331

DeMott CA, Klingaman NP, Woolnough SJ (2015) Atmosphere-ocean coupled processes in the Madden-Julian Oscillation. Rev Geophys 53:1099–1154

Dinku T, Funk C, Peterson P, Maidment R, Tadesse T, Gadain H, Ceccato P (2018) Validation of the CHIRPS satellite rainfall estimates over Eastern of Africa. QJR Meteorol Soc 1:1–21. https://doi.org/10.1002/qj.3244

Diro GT, Grimes DIF, Black E (2011) Teleconnections between Ethiopian summer rainfall and sea surface temperature: Part I. Observation and modelling. Clim Dyn 37:103–119

Donald AM, Meinke H, Power B, Maia AHN, Wheeler MC, White N, Stone RC, Ribbe J (2006) Near-global impact of the Madden-Julian Oscillation on rainfall. Geophys Res Lett 33:L09704. https://doi.org/10.1029/2005GL025155

Eggen M, Ozdogan M, Zaitchik BF, Ademe D, Foltz J, Simane B (2019) Vulnerability of sorghum production to extreme, sub-seasonal weather under climate change. Environ Res Lett 14:045005

Ferranti L, Palmer TN, Molteni F, Klinker E (1990) Tropical extratropical interaction associated with the 30–60 day oscillation and its impact on medium and extended range prediction. J Atmos Sci, 47:2177–2199. https://doi.org/10.1175/1520-0469

Ferranti L, Slingo JM, Palmer TN, Hoskins BJ (1997) Relations between interannual and intraseasonal monsoon variability as diagnosed from AMIP integrations. Q J R Meteorol Soc 123:1323–1357

Funk C, Peterson P, Landsfeld M (2015) The climate hazards infrared precipitation with stations—a new environmental record for monitoring extremes. Sci Data 2:150066. https://doi.org/10.1038/sdata.2015.66

Gill AE (1980) Some simple solutions for heat-induced tropical circulation. Q J Roy Meteor Soc 106:447–462

Gissila T, Black E, Grimes DIF, Slingo JM (2004) Seasonal forecasting of the Ethiopian summer rains. Int J Climatol 24:1345–1358

Gleixner S, Keenlyside N, Viste E, Korecha D (2017) The El Niño effect on Ethiopian summer rainfall. Clim Dyn 49(5–6):1865–1883. https://doi.org/10.1007/s00382-016-3421-z

Hartmann DL, Michelsen ML, Klein SA (1992) Seasonal variations of tropical intraseasonal oscillations: a 20–25 day oscillation in the Western Pacific. J Atmos Sci 49(14):1277–1289

Hidayat R, Kizu S (2010) Influence of the Madden–Julian Oscillation on Indonesian rainfall variability in austral summer. Int J Climatol 30:1816–1825. https://doi.org/10.1002/joc.2005

Higgins RW, Shi W (2001) Intercomparison of the principal modes of interannual and intraseasonal variability of the North American monsoon system. J Clim 14:403–417. https://doi.org/10.1175/1520-0442(2001)014%3c0403:IOTPMO%3e2.0.CO;2

Hsu P, Li T (2012) Role of the boundary layer moisture asymmetry in causing the eastward propagation of the Madden-Julian Oscillation. J Clim 25:4914–4931

Hsu PC, Lee JY, Ha KJ (2016) Influence of Boreal Summer Intraseasonal Oscillation on rainfall extremes in southern China. Int J Climatol 36(3):1403–1412. https://doi.org/10.1002/joc.4433

Jiang X, Li T, Wang B (2004) Structures and mechanisms of the northward-propagating Boreal Summer Intraseasonal Oscillation. J Clim 17:1022–1039

Jones C (2016) The Madden–Julian Oscillation and the monsoons. The monsoons and climate change. Springer, Berlin, pp 207–224

Jones C, Carvalho L (2011) Will global warming modify the activity of the Madden–Julian Oscillation? Q J R Meteorol Soc 137:544–552

Kemball-Cook S, Wang B (2001) Equatorial waves and air-sea interaction in the Boreal Summer Intraseasonal Oscillation. J Clim 14:2923–2942

Kikuchi K, Takayabu YN (2003) Equatorial circumnavigation of moisture signal associated with the Madden-Julian Oscillation MJO during boreal winter. J Meteorol Soc Jpn 44:25–43

Kikuchi K, Wang B, Kajikawa Y (2012) Bimodal representation of the tropical intraseasonal oscillation. Clim Dyn 38:1989–2000

Kim U, Kaluarachchi JJ (2009) Climate change impacts on water resources in the Upper Blue Nile River Basin, Ethiopia. J Am Water Res Assoc 45(6):1361–1378. https://doi.org/10.1111/j.1752-1688.2009.00369.x

Klotzbach PJ (2014) The Madden–Julian oscillation's impacts on worldwide tropical cyclone activity. J Clim 27:2317–2330. https://doi.org/10.1175/JCLI-D-13-00483.1

Knapp K, Ansari S, Bain C, Bourassa M, Dickinson M, Funk C, Huffman G (2011) Globally gridded satellite observations for climate studies. Bull Am Meteorol Soc 92:893–907. https://doi.org/10.1175/2011BAMS3039.1

Korecha D, Barnston AG (2007) Predictability of June–September rainfall in Ethiopia. Mon Weather Rev 135:628–650

Krishnamurti TN, Subramanian D (1982) The 30–50-day mode at 850 mb during MONEX. J Atmos Sci 39:2088–2095

Lau WKM, Waliser DE (eds) (2005) Intraseasonal variability of the atmosphere-ocean climate system. *Springer*, *Heidelberg*

Lavender SL, Matthews AJ (2009) Response of the West African monsoon to the Madden–Julian Oscillation. J Clim 22:4097–4116

Lee J-Y, Wang B, Wheeler MC, Fu X, Waliser DE, Kang I-S (2012) Real-time multivariate indices for the boreal summer intraseasonal oscillation over the Asian summer monsoon region. Clim Dyn 40(1–2):493–509. https://doi.org/10.1007/s00382-012-1544-4

Liebmann B, Smith CA (1996) Description of a complete (interpolated) outgoing longwave radiation dataset. Bull Am Meteorol Soc 77:1275–1277

Lin H, Frederiksen J, Straus D (2019) Sub-seasonal to seasonal prediction: tropical-extratropical interactions and teleconnections. Elsevier, Amsterdam, pp 143–164. https://doi.org/10.1016/B978-0-12-811714-9.00007-3

Lo F, Hendon HH (2000) Empirical extended-range prediction of the Madden–Julian Oscillation. Mon Weather Rev 128:2528–2543. https://doi.org/10.1175/1520-0493

Madden RA (1986) Seasonal-variations of the 40–50-day oscillation in the tropics. J Atmos Sci 43:3138–3158

Madden RA, Julian PR (1971) Detection of a 40–50 day oscillation in the zonal wind in the tropical pacific. J Atmos Sci 28:702–708

Madden RA, Julian PR (1972) Description of global-scale circulation cells in tropics with a 40–50-day period. J Atmos Sci 29:1109–1123

Maloney ED, Kiehl JT (2002) MJO related SST variations over the tropical eastern Pacific during northern Hemisphere summer. J Clim 15:675–689. https://doi.org/10.1175/1520-0442

Mao J, Wu G (2006) Intraseasonal variations of the Yangtze rainfall and its related atmospheric circulation features during the 1991 summer. Clim Dyn 27(7–8):815–830. https://doi.org/10.1007/s00382-006-0164-2

Matthews AJ (2004) Intraseasonal variability over tropical Africa during northern summer. J Clim 17:2427–2440

Mellander PE, Gebrehiwot SG, Gärdenäs AI, Bewket W, Bishop K (2013) Summer rains and dry seasons in the Upper Blue Nile Basin: the predictability of half a century of past and future spatiotemporal patterns. PLOS One. https://doi.org/10.1371/journal.pone.0068461

Mohino E, Janicot S, Douville H, Li LZ (2012) Impact of the Indian part of the summer MJO on west Africa using nudged climate simulations. Clim Dyn 38:2319–2334

Nawaz K, Hussain K, Majeed A, Khan F, Afghan S, Ali K (2010) Fatality of salt stress to plants: morphological, physiological and biochemical aspects. Afr J Biotechnol 9(34):5475–5480

Nogués-Paegle J, Byerle LA, Mo KC (2000) Intraseasonal modulation of South American summer precipitation. Mon Weather Rev, 128:837–850. https://doi.org/10.1175/1520-0493(2000)128

Pohl B, Camberlin P (2006) A typology for intraseasonal oscillations. Int J Climatol 34:430–445

Rauniyar SP, Walsh KJE (2011) Scale interaction of the diurnal cycle of rainfall over the maritime continent and Australia: influence of the MJO. J Clim 24:325–348. https://doi.org/10.1175/2010JCLI3673.1

Recalde-Coronel CG, Zaitchik B, William WP (2019) Madden–Julian oscillation influence on sub-seasonal rainfall variability on the west of South America. Clim Dyn. https://doi.org/10.1007/s00382-019-05107-2

Ren H-L, Ren P (2017) Impact of Madden-Julian Oscillation upon winter extreme rainfall in Southern China: observations and predictability in CFSv2. Atmosphere 8(12):192. https://doi.org/10.3390/atmos8100192

Rui H, Wang B (1990) Development characteristics and dynamic structure of tropical intraseasonal convection anomalies. J Atmos Sci 47:357–379. https://doi.org/10.1175/15200469

Shimizu MH, Ambrizzi T (2016) MJO influence on ENSO effects in precipitation and temperature over South America. Theor Appl Climatol 124:291–301

Sutcliffe JV, Parks YP (1999) The hydrology of the Nile. IAHS Special Publication 5, IAHS, Wallingford, UK

Taye MT, Willems P (2012) Temporal variability of hydroclimatic extremes in the Blue Nile Basin. Water Resour Res. https://doi.org/10.1029/2011WR011466

Teng H, Wang B (2003) Interannual variations of the boreal summer intraseasonal oscillation in the Asian–Pacific region. J Clim 16:3572–3584

Viste E, Sorteberg A (2011) Moisture transport into the Ethiopian highlands. Int J Climatol 33:973–983

Waliser D, Sperber K, Hendon H, Kim D, Maloney E, Wheeler M, Weickmann K, Zhang C, Donner L, Gottschalck J (2008) MJO simulation diagnostics. J Clim 22:3006–3039

Wang B, Xie X (1997) A model for the boreal summer intraseasonal oscillation. J Atmos Sci 54:72–86

Wang B, Webster PJ, Teng H (2005) Antecedents and self-induction of the active-break Indian summer monsoon. Geophys Res Lett 32:L04704. doi:https://doi.org/10.1029/2004GL020996

Wang H, Wang B, Huang F, Ding Q, Lee JY (2012) Interdecadal change of the boreal summer circumglobal teleconnection (1958–2010). *Geophys Res* Lett 39: L12704. https://doi.org/10.1029/2012GL052371

Wang Y, Gozolchiani A, Ashkenazy Y, Havlin S (2016) Oceanic El-Niño wave dynamics and climate networks. New J Phys. https://doi.org/10.1088/1367-2630/18/3/033021

Webster PJ, Magaña VO, Palmer TN, Shukla J, Tomas RA, Yanai M, Yasunari T (1998) Monsoon: processes, predictability and the prospects for prediction. J Geophys Res 103:14451–14510

Wheeler MC, Hendon HH (2004) An all-season real-time multivariate MJO index: development of an index for monitoring and prediction. Mon Weather Rev 132:1917–1932

Wheeler M, Kiladis GN (1999) Convectively coupled equatorial waves: analysis of clouds and temperature in the wavenumber-frequency domain. J Atmos Sci 56:374–399. https://doi.org/10.1175/1520-0469

Wheeler MC, Hendon HH, Cleland S, Meinke H, Donald A (2009) Impacts of the Madden–Julian oscillation on Australian rainfall and circulation. J Clim 22:1482–1498. https://doi.org/10.1175/2008JCLI2595.1

Yang J, Wang B, Bao Q (2010) Biweekly and 21–30-day variations of the subtropical summer monsoon rainfall over the lower reach of the Yangtze River basin. J Clim 23(5):1146–1159. https://doi.org/10.1175/2009jcli3005.1

Yasunari T (1979) Cloudiness fluctuations associated with the northern hemisphere summer monsoon. *J Meteor Soc* Jpn 57:227–242

Zaitchik BF (2017) Madden-Julian Oscillation impacts on tropical African precipitation. Atmos Res 184:88–102. https://doi.org/10.1016/j.atmosres.2016.10.002

Zeleke T, Giorgi F, Mengistu Tsidu G, Diro GT (2013) Spatial and temporal variability of summer rainfall over Ethiopia from observations and a regional climate model experiment. Theor Appl Climatol 111:665–681. DOI https://doi.org/10.1007/s00704-012-0700-4

Zeleke TT, Giorgi F, Diro GT, Zaitchik BF (2017) Trend and periodicity of drought over Ethiopia. Int J Climatol 37:4733–4748

Zhang CD (2005) Madden-Julian oscillation. Rev Geophys 43:RG2003. https://doi.org/10.1029/2004RG000158

Zhu B, Wang B (1993) The 30–60 day convection seesaw between the tropical Indian and western Pacific Ocean. J Atmos Sci 50:184–199

Zhu CW, Nakazawa T, Li JP, Chen LX (2003) The 30–60-day intraseasonal oscillation over the western North Pacific Ocean and its impacts on summer flooding in China during 1998. Geophys Res Lett 30(18):1952. https://doi.org/10.1029/2003GL017817